# A 650 km2 Miocene strewnfield of splash-form impact glasses in the Atacama Desert, Chile

J. Gattacceca, Bertrand Devouard, Jean-Alix J-A Barrat, Pierre Rochette, M.L. Balestrieri, G. Bigazzi, G. Ménard, F. Moustard, E. dos Santos, R. Scorzelli, et al.

Highlights

- Discovery of a ~650 $km^2$ impact glass strewnfield in the Central Depression of the Atacama Desert
- cm-sized splash-form glassy objects, called atacamaites, formed by impact at 7.8±0.26 Ma
- Dacitic composition with the addition of a variable iron meteorite contamination, 5 wt.% on average
- Small size, heterogeneity, oxidation state, contamination level distinguish them from tektites
- Impactor was an iron meteoroid, very likely from the IIAB group

# A 650 km$^2$ Miocene strewnfield of splash-form impact glasses in the Atacama Desert, Chile.

**J. Gattacceca[1], B. Devouard[1], J.-A. Barrat[2], P. Rochette[1], M.L. Balestrieri[3], G. Bigazzi[3†], G. Ménard[1], F. Moustard[1], E. Dos Santos[4], R. Scorzelli[5], M. Valenzuela[6,7], M. Gounelle[8], V. Debaille[9], P. Beck[10], L. Bonal[10], B. Reynard[11], M. Warner[12]**

[1]*CNRS, Aix Marseille Univ, IRD, INRAE, CEREGE, 13545 Aix-en-Provence, France*

[2]*Univ Brest, CNRS, IRD, Ifremer, LEMAR, F-29280 Plouzané, France*

[3]*CNR, Institute of Geosciences and Earth Resources, 56124 Pisa, Italy*

[4]*Instituto de Ciência e Tecnologia, Universidade Federal dos Vales do Jequitinhonha e Mucuri UFVJM, Diamantina, MG 39100-000, Brazil*

[5]*Centro Brasileiro de Pesquisas Físicas – CBPF, Rio de Janeiro, RJ 22290-180, Brazil*

[6] *Departamento de Ciencias Geológicas, Universidad Católica del Norte, Av. Angamos 0610, Antofagasta, Chile*

[7] *Millennium Institute of Astrophysics, Av. Vicuña Mackenna, 4860, Macul, Santiago, Chile*

[8] *Muséum national d'Histoire naturelle, Sorbonne Universités, CNRS, IMPMC, 75005 Paris, France*

[9]*Laboratoire G-Time, Université Libre de Bruxelles, 1050 Brussels, Belgium*

[10]*Univ. Grenoble Alpes, CNRS, IPAG, 38400 Grenoble, France*

[11]*Univ Lyon, ENSL, UCBL, CNRS, LGL-TPE, 69342 Lyon, France*

[12]*NSF National Optical-Infrared Astronomy Research Laboratory, Avda Juan Cisternas 1500, La Serena, Chile.*

## ABSTRACT

Glassy ejecta are associated to a limited number of impact craters, and yet hold key information about hypervelocity impact processes. Here we report on the discovery of a ~650 $km^2$ impact glass strewnfield in the Central Depression of the Atacama Desert. These cm-sized splash-form objects, that we refer to as atacamaites, are essentially composed of a dacitic glass formed by high-temperature melting of local magmatic rocks, with the addition of a variable iron meteorite contamination, 5 wt.% on average. The most likely nature for the impactor is the IIAB iron group. The fission-track plateau method, on two samples, yielded a mean formation age of 7.83±0.26 Ma. No associated impact crater has been discovered so far, suggesting it may be a relatively small, km-sized crater. The glassy nature, aerodynamic shapes, elevated formation temperature, and low water content are reminiscent of tektites. However, their small size, heterogeneity, oxidation state, significant contamination by the impactor, and likely more proximal provenance distinguish them from tektites. Atacamaites have no equivalent among the few known terrestrial ejected impact glasses, and increase the intriguing diversity of such products that we propose to name "tektoids".


## 1. Introduction

Natural silicate glasses generated by hypervelocity impact encompass melts in breccia, and impact glasses *per se*, i.e., individual pieces of glasses with minor proportions of relict unmolten grains or quenched crystals (Dressler and Reimold, 2001; Glass and Simonson, 2013; Koeberl, 2014). Tektites are nearly pure impact glasses ballistically ejected at long distance from their source, and bear typical splash-form shapes. Presently, five tektite strewnfields are recognized (Table 1). Beside tektites, more proximal splash-form impact glasses are found associated with a small number of craters (Table 1). The formation of tektites and other ejected

impact glasses remains largely enigmatic, partly due to their small number of occurrences and variable characteristics. Here we report on the discovery of impact glasses from the Atacama Desert (referred to as "atacamaites").

## 2. Geological setting, strewnfield, macroscopic description

The atacamaite strewnfield is located in the Central Depression of the Atacama Desert between the Coastal Cordillera to the west and the Precordillera (Cordillera Domeyko) to the east. Local rocks are Middle Jurassic to Lower Eocene calc-alkaline volcanic and intrusive rocks present as rocky reliefs and smooth landforms, partly covered unconformably by a thin layer of Upper Miocene-Pliocene alluvial deposits consisting in unconsolidated polymict gravels supported by a sandy matrix deposited between 10 Ma and 1 Ma (Espinoza et al., 2012).

Centimeter-sized dark glassy stones were first noticed in 2011 by one us (MW). Subsequent dedicated field work allowed collecting ~23,000 samples[1] from over 100 discrete locations over a surface of ~650 $km^2$ (Fig. 1). The borders of the strewnfield are constrained by sites where a 60 man.minutes search did not reveal a single atacamaite. A few tens of similar-looking glass samples have been found sporadically about 40 km northwest of the strewnfield. The maximum dimension of the strewnfield is therefore at least 100 km. Samples were encountered lying on the desert surface, and more abundant, up to several tens per $m^2$, in gravels concentrations. They were encountered on all geological units present in the area. They range from 1 to 35 mm in length, with an average mass of 0.55±0.48 g (1$\sigma$), and a maximum mass of 5.9 g. They are pieces of black glass, with minor vesicularity. The vast majority of samples display globular forms, with rare button, dumbbell, or teardrop shapes (Fig. 2A). The average shape parameters L (longest over intermediate axes) and F (intermediate over short axes) are

[1] Research material is available upon request to the first author

1.74±0.57 and 1.43±0.30 (n=989). Most pieces show a somewhat dull abraded surface attributed to transport and/or sand blasting. A limited number of samples show a shiny surface with small droplets stuck to the surface, as well as contorted splash-forms.

## 3. Methods

Optical microscopy was performed with a Leica DM2500P petrographic microscope at CEREGE, France. Backscattered electron (BSE) images, microanalyses by energy dispersive spectroscopy (EDS) and chemical maps were acquired with a Hitachi S3000-N Scanning Electron Microscope (SEM) operated at 15 kV and equipped with a Bruker X-ray XFlash detector and a Spirit analyzer at CEREGE. Semi-quantitative analyses used a variety of natural and synthetic standards.

The grain density was measured with a Quantachrome helium stereopycnometer at CEREGE. Magnetic susceptibility was measured with an Agico MFK1 susceptibility at CEREGE.

Whole-rock major, trace elements and isotopic compositions were determined at the PSO/IUEM (Pôle Spectrométrie Océan, Institut Universitaire Européen de la Mer, Brest, France). 100-150 mg of atacamaites were digested on a hot plate heated to 125°C, using sequential mixtures of HF/$HNO_3$, $HNO_3$ and HCl. The aliquots of the obtained solutions were used for the determination of major and trace element concentrations, Sr and Nd isotopic compositions. Major elements, Ni and Co abundances were analyzed by inductively coupled plasma-atomic emission spectrometry (ICP-AES) using a Horiba Jobin Yvon Ultima spectrometer and following the analytical procedure of Cotten et al. (1995). Relative standard deviations are < 2%. The accuracy is better than 7% for Na and P, and much better than 3% for the other elements. Trace element concentrations were measured with a Thermo® Element2 ICP-SFMS (inductively coupled plasma-sector field mass spectrometer). Concentrations were determined following the procedure described by Barrat et al. (2012, 2016). Based on results obtained on many standards, the reproducibility and accuracy are always better than 5%. Strontium and Nd fractions were prepared following conventional ion exchange techniques. They were analyzed using a Thermo® Triton TIMS (thermal ionization mass spectrometer). Isotopic ratios were normalized against $^{86}Sr/^{88}Sr = 0.1194$ and $^{146}Nd/^{144}Nd=0.7219$. The values

obtained for NBS 987 and La Jolla standards during the course of the study are respectively $^{87}Sr/^{86}Sr = 0.710254 \pm 0.000003$ (2 σ, n=8) and $^{143}Nd/^{144}Nd = 0.511830 \pm 0.000003$ (2 σ, n=6).

Quantitative major element analyses were conducted using electron microprobe analyses (EPMA) Cameca SX100 at UPMC CAMPARIS facility. The operating conditions were 15 kV accelerating voltage with a current of 10 nA and a counting time of 30 s, with a focused beam (1 µm). Both natural and synthetic standards were used for calibration: albite for Na; anorthite for Al; apatite for P; diopside for Mg, Si, Ca; orthoclase for K; $MnTiO_3$ for Mn and Ti; $Fe_2O_3$ for Fe; and NiO for Ni. Typical detection limits are (in ppm): 450 for Na, 470 for Al, 710 for Mg, 670 for Si, 610 for Ca, 600 for K, 1040 for Mn, 420 for Ti, 1270 for Fe, and 1330 for Ni.

$^{57}$Fe Mössbauer spectroscopy ($^{57}$Fe-MS) was conducted at CBPF, Brazil. It was performed at room temperature (RT) in standard transmission geometry using a 25 mCi $^{57}$Co/Rh radioactive source in sinusoidal mode. Spectra were recorded for 96 hours in a 512 channels spectrometer and the drive velocity calibration was taken at room temperature (RT) with an α-Fe foil. All isomer shifts reported in this work are given relative to α-Fe at RT. The error in source velocity is less than 1%. For each studied sample, about 100 mg of material was grinded and used as Mössbauer absorber. Spectral analysis was performed with the two-dimensional extended Voigt-based fitting method (x-VBF) developed by Lagarec and Rancourt (1997). This method provides the total Probability Density Distribution (PDD) of static hyperfine parameters allowing the analysis of independent, partially or fully correlated arbitrary-shape partial distributions of isomer shift (δ), quadrupole splitting (Δ) and, for magnetically ordered materials, hyperfine magnetic Zeeman splitting (z).

Micro-infrared spectroscopy was performed using a Bruker Hyperion Microscope coupled with a Vertex 70 FTIR (Fourier-transform infrared spectroscopy) spectrometer at the Institut de Planétologie et d'Astrophysique de Grenoble, France. Double polished sections of atacamite were prepared with thicknesses in the 300-600 µm range. Transmission spectra were obtained using 32 scans at a spectral resolution of 4 cm-1 for areas of typical size 100 µm x100 µm. The absorbance due to $H_2O$ in the glasses was measured at 3570 $cm^{-1}$ and the water contents were estimated using a Molar Absorptivity of 74.8 L/(mol.cm) (Beran and Koeberl, 1997) and a density of 2430 $kg/m^3$ (as measured by helium pycnometry, see below).

Raman spectra of $SiO_2$ rich inclusions were obtained at Laboratoire de Géologie de Lyon (ENS Lyon, France) using a LabRAM HR800 Evolution spectrometer with a confocal Czerny-Turner geometry and a laser source of 532 nm in wavelength. Spectra were acquired using a

laser power of 10 mW, and 25 accumulations of 5 to 15s. Gratings with 600 groove/mm were used to cover the frequency range 60 to 1300 $cm^{-1}$.

Fission-tracks ages were obtained following the protocol established at the Institute of Geosciences and Earth Resources (IGG-CNR) of Pisa (Laurenzi et al., 2007): samples JG26 and PT7E were handmade crushed to reduced them in multiple pieces. A fraction of each sample was irradiated in the Lazy Susan (Cd ratio 6.5 for Au and 48 for Co) facility of the Triga Mark II reactor of LENA, University of Pavia (Italy). After irradiation, fractions for spontaneous and induced track counting were mounted in epoxy resin, polished, and etched for track revelation (120s in 20% HF at 40°C). Tracks were counted under a Jena-Jenaval microscope with a magnification of 500x. Track-diameters in glass were measured with a magnification of 1000x with a digital tablet. We corrected the obtained ages for track annealing (i.e., track shortening) that occurs even at ambient temperature, and that is revealed by a spontaneous to induced track-diameter ratio $D_S/D_I < 1$ (Storzer and Wagner, 1969). Spontaneous track sizes are reduced by ~ 30 % in JG26 and ~ 20 % in PT7E (Table 4). The correction follows the plateau method which consists in re-establishing, through laboratory thermal treatments, identical etching efficiencies for spontaneous and induced tracks (Storzer and Poupeau, 1973). In this study, following the common practice, only one heating step (4h at 220°C) was used (e.g., Sandhu et al., 1993).

## 3. Petrography

Atacamaites are entirely glassy in the vast majority of cases. They contain a variable proportion (few vol.%) of vesicles ca. 100 µm in diameter. Complex schlieren textures are observed (Figure 2B). Some samples have texture suggesting formation by accretion of molten beads of a few hundreds µm in size (Fig. 2a, Fig. 2c). Lechatelierite (nearly pure silica glass), identified in particular by Raman spectroscopy (Fig. S1), is present as small patches with size ranging from a few µm to more than 2 mm. Some have a whirling texture indicating strong deformation in liquid state (Fig. 2D).

In the most magnetic samples, iron oxides can be observed as dendritic assemblages of micrometer-sized crystallites forming threads or globules (Fig. 2E). These iron oxides were observed only in samples with magnetic susceptibility higher than ~350 $10^{-9}$ $m^3$/kg, which make up 10% of our collection. A few relict grains of incompletely molten quartz were observed in rare samples that were selected among several hundreds because of their abnormal, highly vesicular aspect.

The grain density, measured by helium pycnometry on three separate atacamaite batches totaling 67 g, is 2.48 g/$cm^3$. The water content estimated by micro infrared spectroscopy is 177±32 ppm (19 analyses, on 4 samples).

## 4. Geochemistry

Magnetic susceptibility of atacamaites shows a log normal distribution with a median of 169 $10^{-9}$ $m^3$/kg compatible with a paramagnetic behavior, i.e., iron diluted in the glass (Rochette et al., 2015). Magnetic susceptibility correlates roughly with the bulk Ni content, indicating that it may be a good proxy to select samples with higher extraterrestrial contamination (Rochette et al., 2015). Therefore, in addition to regular samples, we selected specifically samples with high susceptibility (above 300 × $10^{-9}$ $m^3$/kg, and up to 3593 × $10^{-9}$ m3/kg) for bulk major and trace elements analyses, and EPMA.

Average bulk chemical composition of atacamaites (Table 2) is similar to a K-rich dacite, with $SiO_2$ = 64.1 wt.%, $Na_2O+K_2O$ = 6.54 wt.%, and $K_2O$ = 2.98 wt.% (n=15). Iron is extremely heterogeneous ($FeO_{total}$ ranges from 4.58 to 14.2 wt.%), and correlates with Ni and Co abundances that are high, up to 4800 ppm and 400 ppm, respectively (Fig. 3). At microscopic scale, EPMA (Table S1) show that the Fe-rich regions are also enriched in Ni, with a good correlation between Ni and Fe contents (Fig. 3a).

Chondrite-normalized REE patterns are similar for all samples, characterized by a $La_N/Lu_N$ ratio ranging from 7.47 to 8.00 and a significant negative Eu anomaly (Eu/Eu*=0.50), compatible with a dacitic target (Fig. 4). Strontium and Nd isotopic compositions, measured for five samples, also reveal fairly homogeneous isotopic compositions, with $^{87}Sr/^{86}Sr = 0.7076 \pm 0.0001$ and $^{143}Nd/^{144}Nd = 0.512636 \pm 0.000006$ (Fig. 5).

## 5. Mössbauer spectroscopy

Five atacamaite samples were studied for Mössbauer spectroscopy. The room temperature $^{57}Fe$ Mössbauer spectra of all samples were fitted with two components described as distribution 1 (D1) and distribution 2 (D2). A typical spectrum is shown in Figure 6a. Only sample J338-23, selected for its high magnetic susceptibility, exhibited a magnetic phase ordered at room temperature, identified as magnetite and fitted with two sextets assigned as Fe-A and Fe-B. The former, with average hyperfine field ($B_{hf}$) ~ 49 T, corresponds to $Fe^{3+}$ at tetrahedral sites in magnetite while the latter ($B_{hf}$ ~ 45 T) to $Fe^{2.5+}$ at octahedral sites (Cornell and Schwertmann 2003).

Despite the differences in relative areas, all samples exhibit similar average hyperfine parameters for D1 and D2 (Table 3). The main distribution D1 presents average isomer shift $\langle\delta\rangle \sim 0.88 - 1.02$ mm/s and average quadrupole splitting $\langle\Delta\rangle \sim 1.95 - 2.19$ mm/s that is usually associated to $Fe^{2+}$ in octahedral coordination, as shown in previous works on tektites and other natural glasses (Dunlap and Sibley 2004; Stewart et al. 2003). However, as pointed out by Rossano et al. (1999), D1 could also be assigned to a five-fold co-ordinated $Fe^{2+}$. In contrast, distribution D2 with $\langle\delta\rangle \sim 0.49 - 0.56$ mm/s and $\langle\Delta\rangle \sim 0.76 - 0.83$ mm/s is more likely to be $Fe^{3+}$ in octahedral coordination (Johnson and Johnson 2005). Although previous works on tektites (e.g., Australasian) indicate $\langle\Delta\rangle \sim 0.00$ mm/s for $Fe^{3+}$ (Dunlap and Sibley

206 2004), some impact glasses (e.g., Aouelloul glass, irghizites) show iron species with
207 appreciable quadrupole splitting that is very much $Fe^{3+}$-like (Dunlap and McGraw 2007). In
208 this sense, the Mössbauer data of atacamaites have much more in common with these impact
209 glasses. Indeed, except for the presence of magnetite in sample J338-23, the shape of all
210 Mössbauer spectra is very similar to the one of Irghizite impact glass (see Fig. 1c, in Dunlap
211 and McGraw 2007).
212 As shown in Fig. 6b and 6c, the isomer shift and quadrupole splitting for D1 and D2 are
213 distributed around their average values, in accordance with the wide range of local distortion
214 of cation environments observed in glasses. As a result, D1 and D2 may contain small
215 contributions due to tetrahedrally coordinated iron ($Fe^{2+}$ or $Fe^{3+}$), as already identified in
216 silicate glasses (Johnson and Johnson 2005; Stewart et al. 2003). In addition, although the
217 occurrence of electron delocalization has not been reported for previously studied tektites
218 (Rossano et al. 1999), this effect cannot be neglected in our samples - electron delocalization
219 results in average value of isomer shift (0.5 – 0.9 mm/s) that can be assigned to $Fe^{2.5+}$ (Dyar et
220 al. 2006). Despite this issue concerning the distribution of hyperfine parameters, an estimate
221 for $Fe^{3+}$/ $Fe^{2+}$ ratio for the studied samples could be determined if D1 and D2 are associated to
222 $Fe^{2+}$ and $Fe^{3+}$, respectively, based on the average values of hyperfine parameters as previously
223 mentioned. Thus, considering the relative areas for D1 and D2 (Table 3), $Fe^{3+}/Fe^{2+}$ ratio ranges
224 from 0.282 (for sample PT2d) up to 0.857 (for sample J338-23). $Fe^{3+}/Fe_{total}$ can be estimated
225 between 22% (for PT2d) and 36% (for J338-23), taking $Fe_{total} = Fe^{3+} + Fe^{2+}$. The average
226 $Fe^{3+}/Fe_{total}$ ratio is 27.7±5.4% for the three typical atacamaite samples (i.e. the ones with
227 magnetic susceptibility between 176 and 272 $10^{-9}$ $m^3/kg$, namely JG2h, PT2d, and K51f).
228 These ratios are considerably higher than the ones already reported for tektites from other
229 strewnfields, whose $Fe^{3+}$/ $Fe^{2+}$ (or $Fe^{3+}/Fe_{total}$) ratios are close to zero (Dunlap and Sibley 2004;
230 Giuli et al., 2002).

## 6. Dating

The fission-track dating method, applied successfully to a variety of impact glasses (e.g., Folco et al., 2011), was used on two samples collected 3 km apart. The plateau corrected fission-track ages (Storzer and Wagner, 1969) are 8.08±0.54 Ma and 7.57±0.52 Ma (±1σ), consistent within 1σ error, and with an average 7.83±0.26 Ma (Table 4).

## 7. Discussion

### *7.1. Nature of atacamaites*

Petrological and geochemical characteristics of atacamaites, such as the occurrence of lechatelierite that evidence temperatures above 1700°C (Macris et al., 2014) and the low water content (below 200 ppm) exclude a volcanic origin and indicate formation by hypervelocity impact. Such high temperatures may also be reached naturally by lightning, but the morphology, texture and spatial repartition of atacamaites preclude that they are fulgurites. Compositions in major and trace elements, including the REE patterns, suggest a relatively homogeneous lithology for the target rocks, superimposed with a Fe, Ni, and Co extraterrestrial contamination (Fig. 3-5). Although atacamaites and local Andean dacites have whole rock, Sr and Nd isotopic compositions in the same ranges, no lava with exactly the same compositions has yet been identified in the existing database (Oliveiros et al., 2020).

### *7.2. Impactor*

The enrichment in Ni and Co in atacamaites (2148 ppm and 182 ppm, respectively, on average, and up to 4800 ppm and 400 ppm in the most magnetic samples) compared to dacites, and the strong correlation between Fe, Ni and Co contents indicate a significant contamination by an

extraterrestrial impactor rich in Fe, Ni and Co (Fig. 3). Although we do not know the composition of the target, it is necessarily a dacitic rock that has practically no Ni and Co compared to the impactor. Therefore, the Ni/Co ratio of the impactor can be estimated from the Ni/Co ratio of the most impactor-rich atacamaites. This ratio, computed for atacamaites with Ni content above 2500 ppm is Ni/Co=12.0±0.2 (1σ, n=5). The Ni/Co ratio of the impactor (12.0±0.2) is inconsistent with a chondritic projectile characterized by Ni/Co ratios around 21 (e.g., Wasson and Kallemeyn, 1988). Similarly, the absence of enrichment in Cr precludes a chondritic impactor (Fig. 3C). Therefore, the geochemical data point to an iron impactor. Under the reasonable assumption that Fe, Ni, and Co are the only significant elements in the impactor and mixing lines as exemplified in Figure 3, the bulk composition of the impactor is estimated to 94.15 wt.% Fe, 5.4 wt.% Ni, 0.45 wt.% Co.

The 5.4 wt.% Ni content and the 12.0 Ni/Co ratio of the impactor allow to constrain more precisely the nature of the impactor. The only iron meteorite groups with similar Ni content (<7.5 wt.%) are IC, IIAB, and IIG groups with average Ni contents of 6.50±0.27 wt.% (1σ, n=41 analyses), 5.70±0.33 wt.% (n=274), 4.53±0.44 wt.% (n=18), respectively (Koblitz, 2005; Gattacceca et al., 2018, Wasson et al., 2007). The average Ni/Co ratio for IC, IIAB, and IIG meteorites are 14.17±0.68 (n=20), 12.41±0.75 (n=156), 8.97±0.79 (n=8), respectively (Koblitz, 2005; Gattacceca et al., 2018; Wasson et al., 2007). The best fit is clearly with IIAB meteorites. In particular, no IC meteorite has Ni/Co<13.4, and no IIG meteorite has Ni/Co>10.8. Only two meteorites from of the IAB complex, out of 537 analyses, have Ni content below 6 wt.%, and only 5, out of 326 analyses, have Ni/Co <13 (Koblitz, 2005). Therefore, this group is not considered as a candidate impactor for the atacamaites. In conclusion, the IIAB iron group is the most likely candidate for the impactor that formed the atacamaites.

Assuming that all the Ni was provided by the meteorite, an average of 5 wt.% impactor contamination can be estimated for atacamaites (range 0.8 % to 9 %). This elevated

contamination level is in the same range as glasses from small size craters like the 45 m-diameter Kamil crater (Fazio et al., 2016) or the 120 m-diameter Wabar crater (Mittlefeld et al., 1992).

### *7.3. Nomenclature and petrogenesis*

A number of criteria are used to differentiate tektites from other splash-form impact glasses (e.g., Koeberl, 1994). Atacamaites have similarities with tektites: a water content of 177±32 ppm that is similar to the content of 140±80 ppm in tektites (Beran and Koeberl, 1997), distribution over a relatively large strewnfield (similar to ivoirite and belizite strewnfields, Table 1), absence of relict grains or mineral inclusion in most samples.

Atacamaites also have similarities with more proximal splash-form impact glasses. They show small-scale chemical heterogeneities due to a strong contamination by the impactor, while only minor contamination is reported in tektites.

The redox state of Fe determined by Mössbauer spectroscopy in 5 samples, including two very magnetic ones, yields a ratio of $Fe^{3+}/Fe_{total}$ between 22% and 36% (average 27.7±5.4% for the three typical samples). This $Fe^{3+}/ Fe_{total}$ ratio of 27.7±5.4% show that atacamaites are also much more oxidized than tektites whose oxidation ratios are near zero (Table 1). Atacamaites contain Fe oxides inclusions more frequently than tektites where their occurrence is extremely rare. As a consequence, they are more magnetic than tektites, and their magnetic properties are more variable, especially for small specimens (Rochette et al., 2015).

Beside tektites *sensu stricto*, the occurrences of macroscopic splash-form impact glasses, are limited (Table 1). Millimeter-sized ballistic ejecta are found around the Wabar impact craters under the form of glassy droplets (Mittlefeldt et al., 1992), but these are limited to a few hundred meters around three small craters with maximum diameter 120 m (Gnos et al., 2013).

303 Glass with crude splash-forms is also found over limited areas on the rims of the 390 m-
304 diameter Aouelloul crater (Koeberl et al., 1998). Centimeter-sized splash-form glasses are
305 found over a much wider area (~400 $km^2$) around the 1.2 km-diameter Darwin crater (Taylor
306 and Solomon, 1962; Howard, 2009). The impact glasses with closest similarity to atacamaites
307 are irghizites, associated with the 14 km-diameter Zhamanshin crater in Kazakhstan (Bouska
308 et al., 1981). Irghizites and atacamaites share similar morphologies (including presence of
309 small attached spherules, Fig. 2a), and important contamination by the impactor (Schulz et al.,
310 2020). A significant difference is the extent of the strewnfield (1-2 $km^2$ for irghizites vs. 650
311 $km^2$ for Atacamaites).

312 This inventory of tektites and other splash-form impact glasses (Table 1) confirms that it is
313 necessary to combine a number of criteria to discriminate the two categories (following
314 Koeberl, 1994). Chemical homogeneity is a tektite attribute, but it is hard to quantify this
315 homogeneity, and tektites may be heterogeneous (e.g., North American ones, see Albin et al.,
316 2000, and Muong Nong tektites, see Koeberl, 1992). Water content may be ambiguous as non-
317 tektite glasses can be as dry as tektites (Table 1). The reduced character is not exclusive as
318 well, as the Darwin glass is as reduced as tektites (e.g., Rochette et al. 2015). Another criterion
319 may be the distance from the crater that is at least an order of magnitude higher for tektites, but
320 this criterion cannot be strictly applied when the crater location is unknown. A final criterion
321 is crater size, with tektites being associated to craters larger than 10 km. Both criteria cannot
322 be used when the crater is missing, as for atacamaites. In fact, the only other cases of
323 macroscopic non tektite impact glasses without known source crater are Libyan desert glass
324 (e.g., Barrat et al., 1997), and urengoites (e.g., Deutsch et al., 1997), two glasses for which
325 splashforms are not established. The smaller size range (the largest atacamaites are about the
326 size of the smallest tektites) as well as presence of contorted shapes seems to be good criteria
327 for non-tektite material. In addition to the oxidized character and the high impactor

328 contamination observed in atacamaites, this clearly precludes the classification of atacamaites
329 as tektites.

330 *7.4. Source impact crater*

331 Considering our fission track age for the atacamaites (7.83±0.26 Ma) compared to erosion rates
332 < 1 m/Ma measured in the hyper-arid part of the Atacama Desert (e.g., Dunai et al., 2005), a
333 ~10 km diameter (Zhamanshin size) crater and the associated ~400 m deep depression should
334 still be visible in the field and on satellite images. On the other hand, published erosion rates
335 were obtained on surfaces specially selected for their stable morphology. Areas with steep
336 slope or low relative altitude may have higher erosion rates or may have accumulated post 8
337 Ma sediments. Search for impact breccia or non-ejected impact glass were also inconclusive
338 despite several weeks of field work. The failure to detect a candidate source crater for
339 atacamites suggests it may have been much smaller than 10 km, in the size range of Darwin
340 crater (1.2 km diameter) that produced a ~400 $km^2$ strewnfield with ~15% of splash-form
341 (Howard, 2009). Modeling shows that cm-sized particles for such small craters can indeed be
342 ejected for several tens of km (Shuvalov and Dypvik, 2013). Finding such delicate glass ejecta
343 present at the surface of Atacama Desert since nearly 8 Ma points toward the extreme stability
344 of Atacama Desert surfaces, already demonstrated by elevated cosmogenic nuclide contents
345 (Dunai et al., 2015), high meteorite densities (Hutzler et al., 2007), and old meteorite terrestrial
346 ages (Drouard et al., 2019).

347

348 **8. Conclusions**

349 Atacamaites are cm-sized glassy splash-form ejecta found over at least 650 $km^2$ in the Central
350 Depression of the Atacama Desert. They are the product of the fusion and ejection of local
351 andesitic rocks by the hypervelocity impact of an iron meteoroid that occurred at ~7.8 Ma. The

most likely nature of the impactor is the IIAB iron group. No source crater has been identified so far, despite its likely proximal location. Atacamaites do not qualify as tektites *sensu stricto* because of their smaller size, more oxidized character, and high contamination by the impactor.

The discovery of atacamaites adds a new example of a significantly large strewnfield of ejected tektite-like glass that does not meet a number of criteria to qualify as tektite. Following Rochette et al. (2015), we propose to categorize such objects as "tektoids", to shorten the description as "non tektite splash-form impact glasses" and to emphasize their similar aspect to tektites. Better understanding of the specificities of atacamaites should come from finding the source crater or from our ongoing exploration of the variability of atacamaites within their strewnfield (geochemistry, contamination level, size distribution, morphology, …). The characteristics of atacamaites increase the diversity of known impact glasses and hold crucial information to further understand the mechanisms of formation of impact glasses in general, and the consequences of terrestrial impacts on the environment.

## ACKNOWLEDGMENTS

We thank Luigi Folco and an anonymous reviewer for their useful and constructive comments that helped improve this manuscript. This project was funded by the Programme National de Planétologie (INSU/CNES), and FONDECYT (3140562). BR acknowledges financial support of the LABEX Lyon Institute of Origins (ANR-10-LABX-0066) of the Université de Lyon within the program "Investissements d'Avenir" (ANR-11-IDEX-0007) of the French government operated by the National Research Agency (ANR). The national Raman facility at ENS de Lyon is supported by INSU.

## FIGURE CAPTIONS

**Fig. 1**. Map of atacamaite strewnfield. Its estimated limits are indicated by the solid line. Geological information is from Espinoza et al. (2012).

**Fig. 2.** Morphologies and petrography of atacamaites. (a) Macroscopic images. (b) Transmitted light image of a thick section evidencing compositional schlieren and bubbles. (c) Backscatter electron image of a sectioned typical atacamaite. (d) Transmitted plane polarized light image of a lechatelierite inclusion. (e) Backscatter electron image of Fe oxides in a highly magnetic atacamaite.

**Fig. 3.** Atacamaite geochemistry. Ni (a), Co (b), Cr (c) contents vs. Fe content. The linear fits are for ICP-AES data. The fields for pre-Pliocene lavas ($SiO_2$=60-70 wt.%, from Oliveiros et al., 2020) are shown for comparison. Note that no Cr enrichment is apparent, consistent with an iron impactor.

**Fig. 4.** REE concentrations in 12 atacamaites. Concentrations are normalized to CI chondrites (Barrat et al., 2012).

**Fig. 5.** Sr and Nd isotopic compositions of atacamaites compared with those of pre-Pliocene Andean volcanics (Oliveiros et al., 2020).

**Fig. 6.** (a) Room temperature $^{57}$Fe Mössbauer spectrum for atacamaite sample PT7b. (b) Three-dimensional representation of the total probability distribution P(δ, Δ) for PT7B sample as obtained by means of x-VBF method. (c) Contour plots in isomer shift (δ), quadrupole splitting (Δ) plane. For P(δ, Δ) < 0.55, the contour lines are shown as solid lines. For P(δ, Δ) > 0.55, the contour lines are shown as broken lines. All lines are spaced at intervals of 0.11.

## References


Albin, E.F., Norman, M.D., Roden, M. 2000. Major and trace element compositions of georgiaites : clues to the source of North American tektites. Meteorit. Planet. Sci. 35, 795–806.

Anders, E., Grevesse, N., 1989. Abundances of the elements: meteoritic and solar. Geochim. Cosmochim. Acta 53, 197–214.

Barrat, J.-A., Jahn, B.M., Amossé, J., Rocchia, R., Keller, F., Poupeau, G.R., Diemer, E., 1997. Geochemistry and origin of Libyan Desert glasses. Geochim. Cosmochim. Acta 61, 1953–1959.

406 Barrat, J.-A., Zanda, B., Moynier, F., Bollinger, C., Liorzou, C., Bayon, G., 2012.
407 Geochemistry of CI chondrites: Major and trace elements, and Cu and Zn isotopes.
408 Geochim. Cosmochim. Acta 83, 79–92.
409 Barrat, J.-A., Dauphas, N., Gillet, P., Bollinger, C., Etoubleau, J., Bischoff, A., Yamaguchi,
410 A., 2016. Evidence from Tm anomalies for non-CI refractory lithophile element
411 proportions in terrestrial planets and achondrites. Geochim. Cosmochim. Acta, 176, 1–17.
412 Beran, A., Koeberl, C., 1997. Water in tektites and impact glasses by Fourier-transform
413 infrared spectroscopy. Meteorit. Planet. Sci. 32, 211–216.
414 Bigazzi, G., De Michele, V., 1996. New fission-track age determinations on impact glasses.
415 Meteorit. Planet. Sci. 31, 234–236.
416 Bouska, V., Povondra, P., Florenskij, P.V., Randa, Z., 1981. Irghizites and Zhamanshinites:
417 Zhamanshin crater, USSR. Meteoritics 16, 171–1884.
418 Braukmüller, N., Wombacher, F., Heze, D.C., Escoube, R., Münker, C., 2018. The chemical
419 composition of carbonaceous chondrites: Implications for volatile element depletion,
420 complementarity and alteration. Geochim. Cosmochim. Act. 239, 17–48.
421 Chao, E.C.T., Dwornik, E.J., Merrill, C.W., 1966. Nickel-iron spherules from Aouelloul glass.
422 Science 154, 759–760+765.
423 Cornell, R.M., Schwertmann, U., 2003. The iron oxides: structure, properties, reactions,
424 ocurrences and uses. Weinheim, Germany: Wiley-VCH Verlag GmbH & Co. KgaA.
425 Cotten, J., Le Dez, A., Bau, M., Caroff, M., Maury, R., Dulski, P., Fourcade, S., Bohn, M.,
426 Brousse, R., 1995. Origin of rare-earth element and yttrium enrichments in subaerial
427 exposed basalts: evidence from French Polynesia. Chemical Geol. 119, 115–138.
428 Deutsch, A., Ostermann, M., Masaitis, V.L., 1997. Geochemistry and neodymium-strontium
429 isotope signature of tektite-like objects from Siberia (urengoites, South-Ural glass).
430 Meteorit. Planet. Sci. 32, 679–686.
431 Dressler, B.O., Reimold, W.U., 2001. Terrestrial impact melt rocks and glasses. Earth Sci. Rev.
432 56, 205-284.
433 Drouard, A., Gattacceca, J., Hutzler, A., Rochette, P., Braucher, R., Bourlès, D., ASTER Team,
434 Gounelle, M., Morbidelli, A., Debaille, V., Van Ginneken, M., Valenzuela, M., Quesnel,

435 Y., Martinez, R., 2019. The meteorite flux of the past 2 m.y. recorded in the Atacama
436 Desert. Geology 47, 673–676.
437 Dunlap, R.A., Sibley, A.D.E., 2004. A Mössbauer effect study of Fe-site occupancy in
438 Australasian tektites. J. Non-Crystalline Solids 337, 36–41.
439 Dunlap, R.A., McGraw, J.D., 2007. A Mössbauer effect study of Fe environments in impact
440 glasses. J. Non-Crystalline Solids 353, 2201–2205.
441 Dyar, M.D., Agresti, D.G., Schaefer, M.W., Grant, C.A., Sklute, E.C., 2006. Mössbauer
442 spectroscopy of earth and planetary materials. Annual Rev. Earth and Planet. Sci. 34, 83-
443 125.
444 Espinoza, F.G., Matthews, S.J., Cornejo P.P., 2012. Carta Los Vientos, Región de Antofagasta.
445 Servicio Nacional de Geología y Minería, Carta Geológica de Chile, Serie Geología Básica
446 138: 72 p., scale 1:100.000. Santiago.
447 Fazio, A., D'Orazio, M., Cordier, C., Folco, L., 2016. Target-projectile interaction during
448 impact melting at Kamil Crater, Egypt. Geochim. Cosmochim. Acta 180, 33–50.
449 Folco, L., Bigazzi, G., D'Orazio, M., Balestrieri, M.L., 2011. Fission track age of
450 Transantarctic Mountain microtektites. Geochim. Cosmochim. Acta 75, 2356–2360.
451 Gattacceca, J., Bouvier, A., Grossman, J., Metzler, K., Uehara, M. 2018. The Meteoritical
452 Bulletin, No 106. Meteorit. Planet. Sci. 54, 469–471.
453 Gentner, W., Storzer, D. Wagner, G.A., 1969. New fission track ages of tektites and related
454 glasses. Geochim. Cosmochim. Acta 33, 1075–1081.
455 Giuli, G., Pratesi, G., Cipriani, C., Paris, E., 2002. Iron local structure in tektites and impact
456 glasses by extended X-ray absorption fine structure and high-resolution X-ray absorption
457 near-edge structure spectroscopy. Geochim. Cosmochim. Acta 66, 4347–4353.
458 Gnos, E., Hofmann, B.A., Halawani, M.A., Tarabulsi, Y., Hakeem, M., Al Shanti, M., Greber,
459 N.D., Holm, S., Alwmark, C., Greewood, R.C., Ramseyer, K., 2013. The Wabar impact
460 craters, Saudi Arabia, revisited. Meteorit. Planet. Sci. 48, 2000–2014.
461 Haines, P.W., Jenkins, R.J., Kelley, S.P., 2001. Pleistocene glass in the Australian desert: the
462 case for an impact origin. Geology 29, 899–902.

Howard, K.T., 2009. Physical distribution trends in Darwin glass. Meteorit. Planet. Sci. 44, 115–129.

Hutzler, A., Gattacceca, J., Rochette, P., Braucher, R., Carro, B., Christensen, E., Cournède, C., Gounelle, M., Laridhi-Ouazaa, N., Martinez, R., Warner, M., Bourlès, D., 2016. Description of a very dense meteorite collection area in western Atacama: insight into the long-term composition of the meteorite flux to Earth. Meteorit. Planet. Sci. 51, 468–482.

Johnson, J.A., Johnson, C.E., 2005. Mössbauer spectroscopy as a probe of silicate glasses. J. Physics: Condensed Matter 17, R381–R412.

Koeberl, C. 1992. Geochemistry and origin of Muong Nong-type tektites. Geochim. Cosmochim. Acta 56:1033–1064.

Koeberl, C., 1994. Tektite origin by hypervelocity asteroidal or cometary impact. Target rocks, source craters, and mechanisms, *in* Dressler, B.O., Grieve, R.A.F., and Sharpton, V.L., eds., Large Meteorite Impacts and Planetary Evolution: Geological Society of America Special Paper 293, p. 133-152.

Koeberl, C., 2014. The Geochemistry and Cosmochemistry of Impacts, in Planets, Asteroids, Comets and The Solar System, *in* Andrew M. Davis, ed., Treatise on Geochemistry (Second Edition), v. 2, p.73-118.

Koeberl, C., Bottomley, R., Glass, B.P., Storzer, D., 1997. Geochemistry and age of Ivory Coast tektites and microtektites. Geochim. Cosmochim. Acta 61, 1745–1772.

Koeberl, C., Reimold, W.U., Shirey, S.B., 1998. The Aouelloul crater, Mauritania: on the problem of confirming the impact origin of a small crater. Meteorit. Planet. Sci. 33, 513–517.

Koeberl, C., Crosta, A.P., Schulz, T., 2019. Geochemical investigation of the atacamaites, a new impact glass occurrence in South America. 50$^{th}$ Lunar Planet. Sci. Conf., abstract 1255.

Koblitz, J. 2005. MetBase – Meteorite Data Retrieval Software, version 7.1. Bremen, Germany (CD-ROM).

Lagarec, K., Rancourt, D.G. 1997. Extended Voigt-based analytic lineshape method for determining N-dimensional correlated hyperfine parameter distributions in Mössbauer spectroscopy. Nuclear Instruments Methods Phys. Res. Section B 126, 266–280.

Laurenzi, A., Balestrieri, M.L., Bigazzi, G., Hadler Neto, J.C., Iunes, P.J., Norelli, P., Oddone, M., Osorio Araya, A.M., Viramonte, J.G., 2007. New constraints on ages of glasses proposed as reference materials for fission-track dating. Geostandards Geoanalytical Res. 31, 105–124.

Macris, C.A., Asimow, P.D., Badro, J., Eiler, J.M., Zhang, Y., Stolper, E.M., 2018. Seconds after impact: Insights into the thermal history of impact ejecta from diffusion between lechatelierite and host glass in tektites and experiments. Geochim. Cosmochim. Acta 241, 69–94.

Magna, T., Zak, K., Pack, A., Moynier, F., Mougel, B., Peters, S., Skala, R., Jonasova, S., Mizera, J., Randa, Z., 2017. Zhamanshin astrobleme provides evidence for carbonaceous chondrite and post-impact exchange between ejecta and Earth's atmosphere. Nature Communications 88, article no. 227.

Murali, A.V., Zolensky, M.E., Blanchard, D.P., 1987. Tektite-Like Bodies at Lonar Crater, India, Implications for the Origin of Tektites. J. Geophys. Res. 92, no. B4, E729–E735.

Mittlefehldt, D.W., See, T.H., Hörz, F., 1992. Dissemination and fractionation of projectile materials in the impact melts from Wabar Crater, Saudi Arabia. Meteoritics 27, 361–370.

Oliveros, V., Moreno-Yaeger, P., Flores, L., 2020. Igneous Rock Associations 25. Pre-Pliocene Andean Magmatism in Chile. Geoscience Canada, 47, 65–82.

Osinski, G.R., Kieniewicz, J., Smith, J.R., Bosloughb, M., Eccleston, M., Scharcz, H.P., Kleindienst, M.R., Haldemann, A.F.C., Churcher, C.S., 2008. The Dakhleh Glass: Product of an impact airburst or cratering event in the Western Desert of Egypt? Meteorit. Planet. Sci. 43, 2089–2107.

Rochette, P., Gattacceca, J., Devouard, B., Moustard, F., Bezaeva, N., Cournède, C., Scaillet, B., 2015. Magnetic properties of tektites and other related impact glasses. Earth Planet. Sci. Lett. 432, 381–390.

Rochette, P., Bezaeva, N., Kosterov, A., Gattacceca, J., Masaitis, V., Badyukov, D.D., Giuli, G., Lepore, G.O., Beck, P., 2019. Magnetic Properties and Redox State of Impact Glasses: A Review and New Case Studies from Siberia. Geosciences 9, article no. 225.

Rochette, P., Beck, P., Braucher, R., Cornec, J., Debaille, V., Devouard, B., Gattacceca, J., Jourdan, F., Moustard, F., Moynier, F., Nomade, S., Reynard, B., 2021. A new tektite strewn-field and source crater couple discovered in Central America: insights into the tektite generation process and its ubiquity. Commun. Earth Environ. 2, 94. Doi:10.1038/s43247-021-00155-1.

Roperch, P., Gattacceca, J., Valenzuela, M., Devouard, B., Lorand, J.-P., Arriagada, C., Rochette, P., Latorre, C., Beck, P., 2017. Surface vitrification caused by natural fires in Late Pleistocene wetlands of the Atacama desert. Earth and Planetary Science Letters 469, 15–26.

Rossano, S., Balan, E., Morin, G., Bauer, J.P., Calas, G., Brouder, C., 1999. $^{57}$Fe Mössbauer spectroscopy of tektites. Phys. Chem. Minerals 26, 530–538.

Sandhu, A.S., Westgate, J.A., Alloway, B.V., 1993. Optimizing the isothermal plateau fission-track dating method for volcanic glass shards. Nuclear Tracks Radiation Measurements 21, 479–488.

Schulz, T., Sackl, F., Fragner, E., Luguet, A., van Acken, D., Begosew, A., Badjukov, D.D., Koeberl, C., 2020. The Zhamanshin impact structure, Kazakhstan: A comparative geochemical study of target rocks and impact glasses. Geochim. Cosmochim. Acta 268, 209–229.

Schultz, P.H., Zárate, M., Hames, B., Koeberl, C., Bunch, T., Storzer, D., Renne, P., Wittke, J., 2004. The Quaternary impact record from the Pampas, Argentina. Earth Planet. Sci. Lett. 219, 221–238.

Shuvalov, V., Dypvik, H., 2013, Distribution of ejecta from small impact craters. Meteorit. Planet. Sci. 48, 1034–1042.

Stewart, S.J., Cernicchiaro, G., Scorzelli, R.B., Poupeau, G., Acquafredda, P., De Francesco, A., 2003. Magnetic properties and $^{57}$Fe Mössbauer spectroscopy of Mediterranean prehistoric obsidians for provenance studies. J.Non-Crystalline Solids 323, 188–192.

Storzer, D., Wagner, G.A., 1970. Fission track ages and ages of deposition of deep-sea microtektites. Science 168, 359–361.

Storzer, D., Poupeau, G., 1973. Ages-plateau de minéraux et verres par la méthode des traces de fission. C. R. de l'Académie des Sciences Paris 276 (D), 317–319.

Storzer, D., Wagner, G.A., 1969. Correction of thermally lowered fission-track ages of tektites. Earth Planet. Sci. Letters 5, 463–468.

Taylor, S.R., Solomon, M., 1962. Geochemical and geological evidence for the origin of Darwin glass. Nature 196, 124–126.

Wasson, J.T., Kallemeyn, G.W., 1988. Compositions of chondrites. Philosoph. Transactions Royal Society London A325, 535–544.

Wasson, J.T., Huber, H., Malvin, D.J., 2007. Formation of IIAB iron meteorites. Geochim. Cosmochim. Acta 71, 760–781.

559 **TABLES**

560 **Table 1**. Characteristics of known splash-form impact glasses.

| | $Fe^{3+}/Fe_{total}$ | water (ppm) | magnetic susceptibility ($10^{-9}$ $m^3/kg$) mean±SD | range | maximum distance from crater (km) | crater diameter (km) | age (Ma) | impactor |
|---|---|---|---|---|---|---|---|---|
| Australasian* | <0.1 | 156±76 | 82±10 | 73-129 | ≥5000 | ? | 0.788 | ordinary chondrite? |
| belizites* | <0.1 | 99±31 | 127±5 | 112-193 | 530 | 14 | 0.8 | ordinary chondrite |
| ivoirites* | <0.1 | 23±5 | 103±12 | 62-138 | 320 | 10.5 | 1.1 | L ordinary chondrite |
| moldavites* | <0.1 | 83±17 | 31±19 | 25-60 | 600 | 24 | 14.9 | achondrite? |
| North-American* | <0.1 | 183+77 | 65±24 | 43-129 | 2300 | 85 | 35.5 | chondrite? |
| Wabar glass | 0.2 | ? | 468±58 | 125-1025 | 1.3 | 0.12 | 0.005 | IIIAB |
| Darwin glass | <0.1 | 470 | 53±23 | 34-79 | 35 | 1.2 | 0.73 | ? |
| irghizites | 0.2-0.4 | 283±173 | 164±59 | 45-3320 | 0 | 13.5 | 0.9 | carbonaceous chondrite |
| Aouelloul glass | 0.3 | 350±20 | 82±9 | 38-463 | 0 | 0.36 | 3.1 | Iron (IIB, IIID?) |
| **atacamaites** | **0.28±0.05** | **177±32** | **191±71** | **84-20500** | **≥50** | **?** | **7.6** | **Iron (IIAB)** |

561 Tektites, indicated by *, and other glasses are listed by increasing age. Other glasses are by
562 alphabetical order. Non-ejected glasses tentatively attributed to impact or airbursts such as
563 Dahkleh (Osinski et al., 2008), Argentinian (Schultz et al., 2004), and Edeowie glasses (Haines
564 et al., 2001) are not listed, also because an alternative formation mechanism by fire and
565 associated surface melting has been proposed for such glasses (Roperch et al., 2017). Magnetic
566 properties from Rochette et al. (2015). Crater diameters, age, maximum distance and impactor
567 type are mostly from Dressler and Reimold (2001) and Koeberl (2014). $Fe^{3+}/Fe_{total}$ are from
568 Rochette et al. (2019). Water content are mostly from Beran and Koeberl (1997). Other
569 references used: Howard (2009) for Darwin glass, Gnos et al. (2013) for Wabar glass, Magna
570 et al. (2017) for irghizites, Rochette et al. (2021) for belizites.

571 **Table 2.** Major and trace element abundances of atacamaites (oxides in wt.%, others in ppm).

| # | K48k | K51j | K51f | JG2h | PT7e | PT3i | JG2a | PT7b | K51b | PT3b | PT2d | PT2g |
|---|---|---|---|---|---|---|---|---|---|---|---|---|
| χ | 188 | 133 | 272 | 176 | 91 | 1038 | 136 | 3593 | 167 | 168 | 132 | 147 |
| $SiO_2$* | 64.3 | 66.4 | 60.1 | 64.5 | 68.1 | 58.2 | 65.8 | 60.2 | 64.1 | 64.7 | 66.2 | 66.3 |
| $TiO_2$ | 0.52 | 0.53 | 0.54 | 0.52 | 0.54 | 0.64 | 0.52 | 0.50 | 0.52 | 0.52 | 0.52 | 0.52 |
| $Al_2O_3$ | 12.72 | 12.99 | 13.28 | 12.51 | 13.36 | 15.91 | 12.89 | 12.13 | 12.83 | 12.54 | 12.84 | 12.67 |
| FeO | 9.09 | 6.88 | 11.89 | 9.27 | 4.58 | 9.64 | 7.06 | 14.18 | 9.38 | 8.87 | 7.28 | 7.40 |
| MnO | 0.08 | 0.08 | 0.08 | 0.07 | 0.08 | 0.10 | 0.08 | 0.07 | 0.08 | 0.08 | 0.07 | 0.07 |
| MgO | 1.91 | 1.84 | 1.45 | 1.98 | 2.44 | 2.06 | 1.98 | 1.53 | 1.95 | 1.91 | 1.99 | 1.96 |
| CaO | 4.45 | 4.32 | 5.57 | 4.34 | 4.45 | 5.37 | 4.64 | 4.87 | 4.34 | 4.43 | 4.36 | 4.35 |
| $Na_2O$ | 3.58 | 3.60 | 3.54 | 3.52 | 3.37 | 4.12 | 3.71 | 3.19 | 3.47 | 3.56 | 3.53 | 3.57 |
| $K_2O$ | 2.91 | 3.06 | 2.94 | 2.91 | 2.97 | 3.55 | 3.05 | 2.67 | 2.88 | 2.98 | 2.89 | 2.89 |
| $P_2O_5$ | 0.10 | 0.09 | 0.07 | 0.08 | 0.06 | 0.09 | 0.06 | 0.08 | 0.07 | 0.10 | 0.07 | 0.06 |
| Co | 224 | 133 | 311 | 222 | 45 | 208 | 144 | 409 | 217 | 212 | 150 | 159 |
| Ni | 2735 | 1545 | 3838 | 2636 | 412 | 2242 | 1703 | 4803 | 2584 | 2550 | 1697 | 1780 |
| Li | 49.34 | 53.38 | 56.46 | 49.86 | 52.77 | 64.29 | 48.11 | 46.57 | 46.65 | 50.66 | 48.14 | 48.85 |
| Be | 1.96 | 2.10 | 2.12 | 1.96 | 2.14 | 2.55 | 1.92 | 1.78 | 1.86 | 1.99 | 1.95 | 1.99 |
| Sc | 9.73 | 9.85 | 9.76 | 9.66 | 10.02 | 11.46 | 9.26 | 8.82 | 9.50 | 9.88 | 9.62 | 9.58 |
| V | 85.58 | 83.73 | 86.29 | 83.25 | 75.67 | 91.17 | 81.14 | 74.77 | 80.81 | 89.26 | 79.34 | 81.44 |
| Cr | 34.38 | 27.06 | 30.11 | 35.02 | 18.77 | 29.25 | 27.99 | 29.47 | 32.28 | 34.03 | 27.45 | 28.64 |
| Cu | 14.29 | 12.19 | 16.77 | 11.88 | 3.78 | 13.15 | 12.06 | 15.24 | 12.27 | 17.11 | 10.29 | 12.10 |
| Zn | 10.41 | 7.07 | 10.81 | 6.15 | 3.93 | 9.51 | 5.96 | 8.78 | 7.03 | 12.87 | 6.63 | 7.36 |
| Ga | 14.36 | 12.36 | 16.10 | 12.34 | 7.46 | 13.73 | 13.14 | 14.33 | 12.85 | 16.07 | 11.78 | 12.37 |
| Rb | 97.66 | 98.71 | 99.40 | 90.15 | 83.82 | 112.62 | 94.86 | 84.68 | 91.76 | 102.95 | 92.60 | 95.04 |
| Sr | 226 | 231 | 255 | 214 | 228 | 283 | 220 | 227 | 221 | 230 | 214 | 223 |
| Y | 38.74 | 39.78 | 38.54 | 38.37 | 41.52 | 47.67 | 37.45 | 33.99 | 37.63 | 39.59 | 38.34 | 38.66 |
| Zr | 178 | 178 | 195 | 172 | 175 | 231 | 167 | 167 | 168 | 180 | 169 | 172 |
| Nb | 11.41 | 11.13 | 11.83 | 11.03 | 11.55 | 13.56 | 10.66 | 10.30 | 10.62 | 11.38 | 10.77 | 10.91 |
| Cs | 5.48 | 5.28 | 4.98 | 4.89 | 4.25 | 5.71 | 6.26 | 5.29 | 5.96 | 6.81 | 5.95 | 6.02 |
| Ba | 635 | 650 | 631 | 616 | 723 | 769 | 623 | 589 | 624 | 652 | 552 | 633 |
| La | 37.12 | 38.35 | 36.30 | 36.67 | 41.85 | 45.59 | 36.61 | 33.35 | 36.70 | 38.45 | 36.90 | 37.60 |
| Ce | 69.61 | 74.78 | 72.30 | 69.17 | 77.76 | 88.96 | 69.59 | 65.65 | 69.13 | 73.32 | 70.12 | 70.82 |
| Pr | 8.18 | 8.86 | 8.40 | 8.30 | 9.18 | 10.35 | 8.34 | 7.60 | 8.26 | 8.73 | 8.32 | 8.47 |
| Nd | 31.79 | 34.39 | 32.79 | 32.33 | 35.22 | 40.82 | 32.42 | 29.40 | 32.22 | 33.92 | 32.44 | 32.81 |
| Sm | 6.67 | 6.94 | 6.77 | 6.68 | 7.45 | 8.38 | 6.61 | 6.03 | 6.63 | 7.01 | 6.67 | 6.74 |
| Eu | 1.09 | 1.07 | 1.07 | 1.08 | 1.13 | 1.31 | 1.05 | 0.95 | 1.07 | 1.12 | 1.06 | 1.08 |
| Gd | 6.53 | 6.14 | 6.12 | 6.30 | 6.71 | 7.60 | 6.12 | 5.52 | 6.19 | 6.54 | 6.27 | 6.25 |
| Tb | 1.02 | 0.96 | 0.95 | 0.98 | 1.05 | 1.19 | 0.96 | 0.87 | 0.97 | 1.02 | 0.98 | 0.99 |
| Dy | 6.09 | 5.84 | 5.70 | 5.98 | 6.54 | 7.16 | 5.79 | 5.29 | 5.92 | 6.26 | 5.99 | 6.00 |
| Ho | 1.24 | 1.22 | 1.18 | 1.24 | 1.37 | 1.50 | 1.20 | 1.10 | 1.23 | 1.30 | 1.25 | 1.26 |
| Er | 3.52 | 3.53 | 3.42 | 3.58 | 4.01 | 4.31 | 3.51 | 3.21 | 3.55 | 3.70 | 3.59 | 3.59 |

| | | | | | | | | | | | | |
|---|---|---|---|---|---|---|---|---|---|---|---|---|
| Yb | 3.37 | 3.60 | 3.42 | 3.48 | 3.86 | 4.33 | 3.47 | 3.19 | 3.44 | 3.61 | 3.50 | 3.52 |
| Lu | 0.49 | 0.54 | 0.50 | 0.51 | 0.56 | 0.63 | 0.51 | 0.47 | 0.50 | 0.53 | 0.51 | 0.51 |
| Hf | 4.89 | 5.38 | 5.71 | 4.98 | 5.20 | 6.62 | 5.09 | 4.99 | 4.97 | 5.32 | 5.04 | 5.04 |
| Ta | 0.88 | 0.95 | 0.99 | 0.89 | 0.94 | 1.15 | 0.90 | 0.86 | 0.87 | 0.94 | 0.89 | 0.89 |
| Pb | 3.12 | 2.25 | 2.92 | 1.65 | 1.25 | 2.52 | 2.09 | 1.66 | 2.42 | 2.65 | 1.70 | 1.90 |
| Th | 11.42 | 10.98 | 11.41 | 11.25 | 12.28 | 13.73 | 11.21 | 10.70 | 11.36 | 12.21 | 11.43 | 11.35 |
| U | 1.91 | 1.80 | 1.51 | 1.92 | 1.73 | 1.92 | 1.92 | 1.39 | 1.87 | 2.18 | 1.85 | 1.83 |

572 $\chi$: magnetic susceptibility in $10^{-9}$ $m^3/kg$. *$SiO_2$ was not measured and obtained by difference
573 assuming a total of 100 wt.%.
574

**Table 3.** Room temperature $^{57}$Fe hyperfine parameters for atacamaite samples

| Samples | D1 | | | D2 | | | Magnetite | | | | | | | | Area ratio |
|---|---|---|---|---|---|---|---|---|---|---|---|---|---|---|---|
| | | | | | | | Fe-A | | | | Fe-B | | | | |
| | <δ> (mm/s) | <Δ> (mm/s) | A (%) | <δ> (mm/s) | <Δ> (mm/s) | A (%) | <δ> (mm/s) | <Δ> (mm/s) | <$B_{hf}$> (T) | A (%) | <δ> (mm/s) | <Δ> (mm/s) | <$B_{hf}$> (T) | A (%) | D2/D1 |
| PT7b | 1.02 | 2.07 | 64 | 0.52 | 0.83 | 36 | - | - | - | - | - | - | - | - | 0.56 |
| JG2h | 1.00 | 2.00 | 74 | 0.56 | 0.80 | 26 | - | - | - | - | - | - | - | - | 0.35 |
| PT2d | 0.99 | 1.95 | 78 | 0.53 | 0.79 | 22 | - | - | - | - | - | - | - | - | 0.28 |
| K51f | 0.93 | 2.10 | 65 | 0.53 | 0.76 | 35 | - | - | - | - | - | - | - | - | 0.54 |
| J338-23 | 0.88 | 2.19 | 42 | 0.49 | 0.78 | 36 | 0.32 | -0.01 | 48.6 | 14 | 0.70 | -0.08 | 44.7 | 8 | 0.86 |

<δ>: mean isomer shift relative to alpha-iron, <Δ>: mean quadrupole splitting, <$B_{hf}$>: mean hyperfine field, A: relative area. The Gaussian widths for the center shift ($\sigma_\delta$) and quadrupole splitting ($\sigma_\Delta$) distributions range from 0.15 to 0.30 and 0.15 to 0.43, respectively. The correlation parameter for the x-VBF method are taken to be 0.01 and 0.07 for the D1 and D2 distributions, respectively. Typical uncertainties for <δ>, <Δ>, and <$B_{hf}$> are ±2 for the last digit. For relative area, uncertainty is ±1%.

**Table 4**. Fission-track dating

| Sample | Heating | $\rho_S$ ($cm^{-2}$) | $n_S$ | $\rho_I$ ($cm^{-2}$) | $n_I$ | $p(\chi^2)$ (%) | $D_S/D_I$ | Age (± 1σ) (Ma) |
|---|---|---|---|---|---|---|---|---|
| JG26 | Ambient | 1990 | 66 | 183000 | 1071 | 66 | 0.72 | 3.42 ± 0.43 |
| | 4h 220°C | 1400 | 282 | 54700 | 1084 | 7 | 1.01 | 8.08 ± 0.54 |
| PT7E | Ambient | 2370 | 329 | 177000 | 1041 | 99 | 0.83 | 4.20 ± 0.27 |
| | 4h 220°C | 1680 | 260 | 70100 | 1108 | 60 | 0.97 | 7.57 ± 0.52 |

Heating: Thermal treatment imposed for plateau age determination; $\rho_S$ ($\rho_I$): spontaneous (induced) track density; $n_S$ ($n_I$): spontaneous (induced) tracks counted; p ($\chi^2$): probability of obtaining $\chi^2$ value testing induced track counts against a Poisson distribution; $D_S/D_I$: spontaneous to induced track-size ratio. Parameters used for age calculation: $\lambda = 1.55125 \times 10^{-10}$ $a^{-1}$; $\lambda_F = 8.46 \times 10^{-17}$ $a^{-1}$; $\sigma = 5.802 \times 10^{-22}$ $cm^2$; $^{238}U/^{235}U = 137.88$. Samples were irradiated in the Lazy Susan (Cd ratio 6.5 for Au and 48 for Co) facility of the Triga Mark II reactor of L.E.N.A., University of Pavia, Italy. The neutron fluence, $\Phi = 5.26 \times 10^{15}$ $cm^{-2}$, was determined using the NRM IRMM-540 standard glass. Age errors are propagation of Poisson counting errors.

Fig 2

Click here to access/download;Figure;Fig 2-petrography.tif

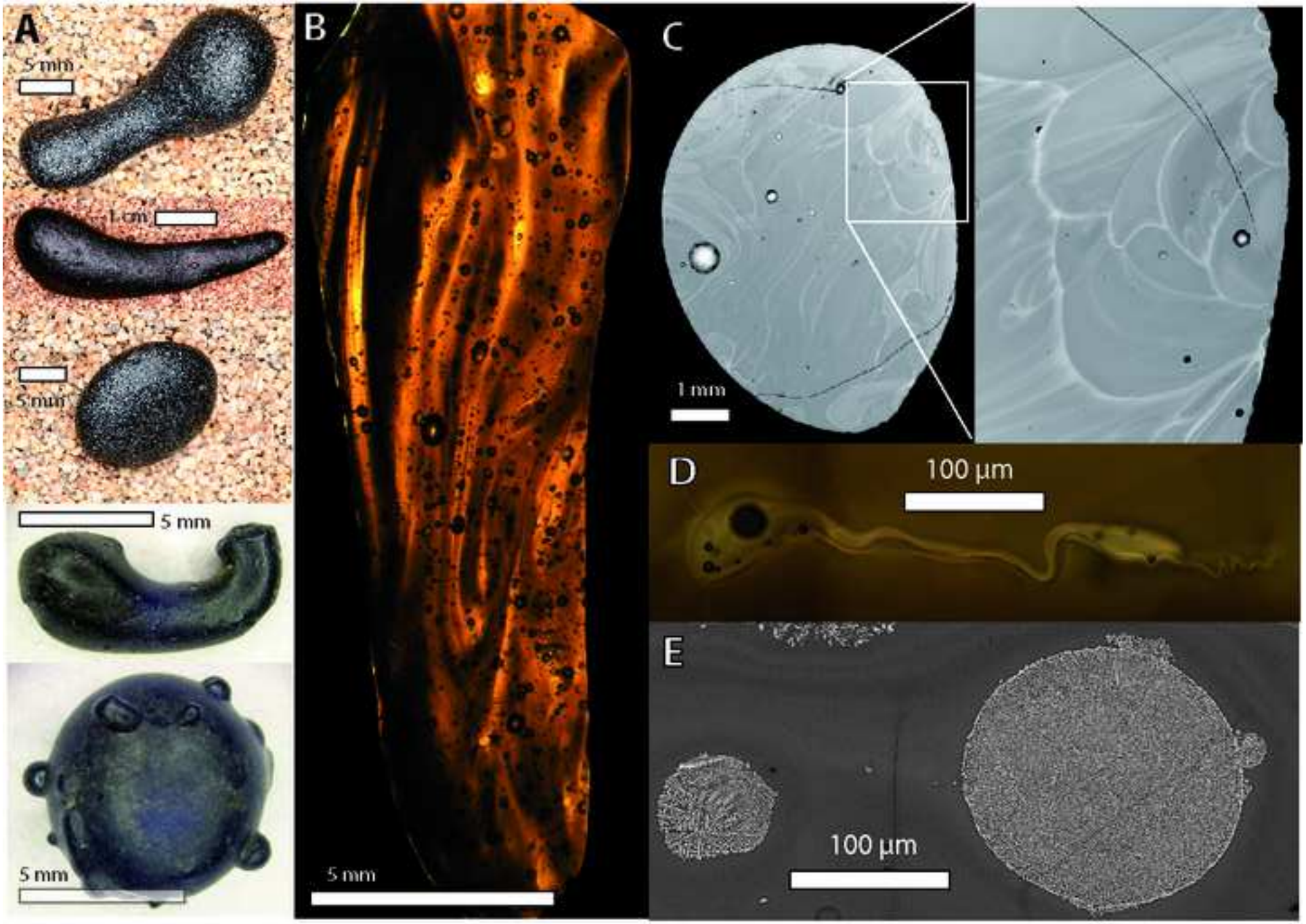

Fig 4



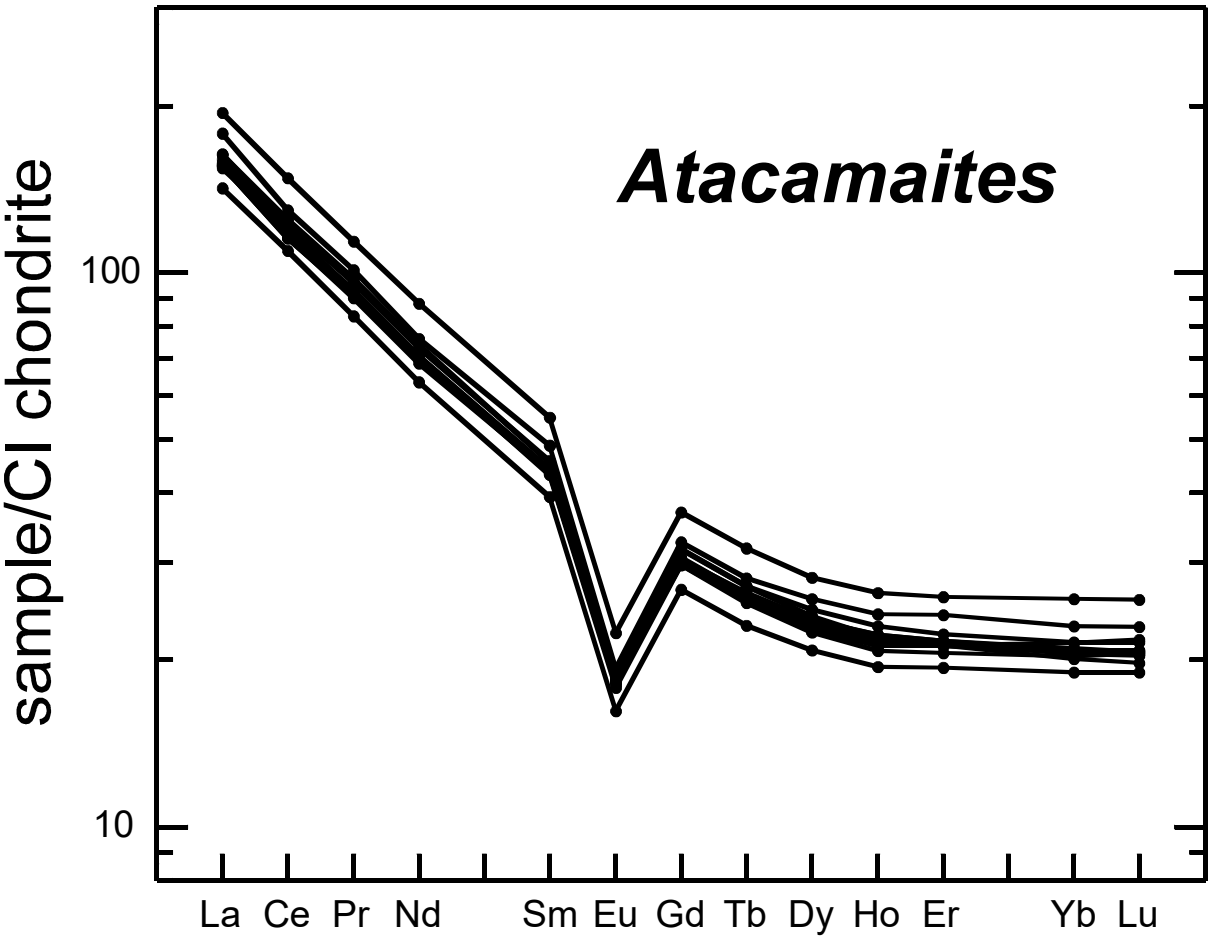

Fig 5



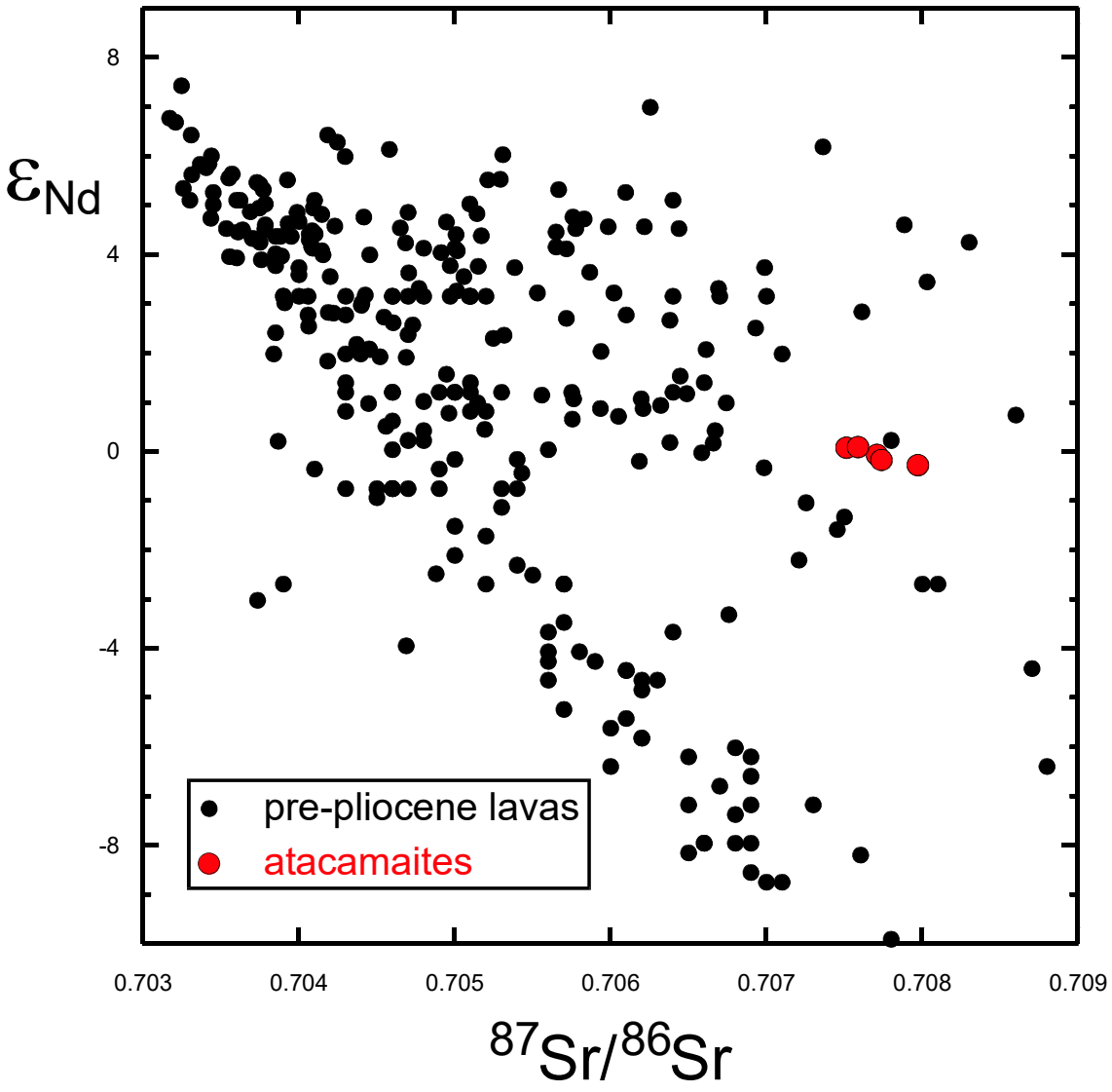

Fig 6



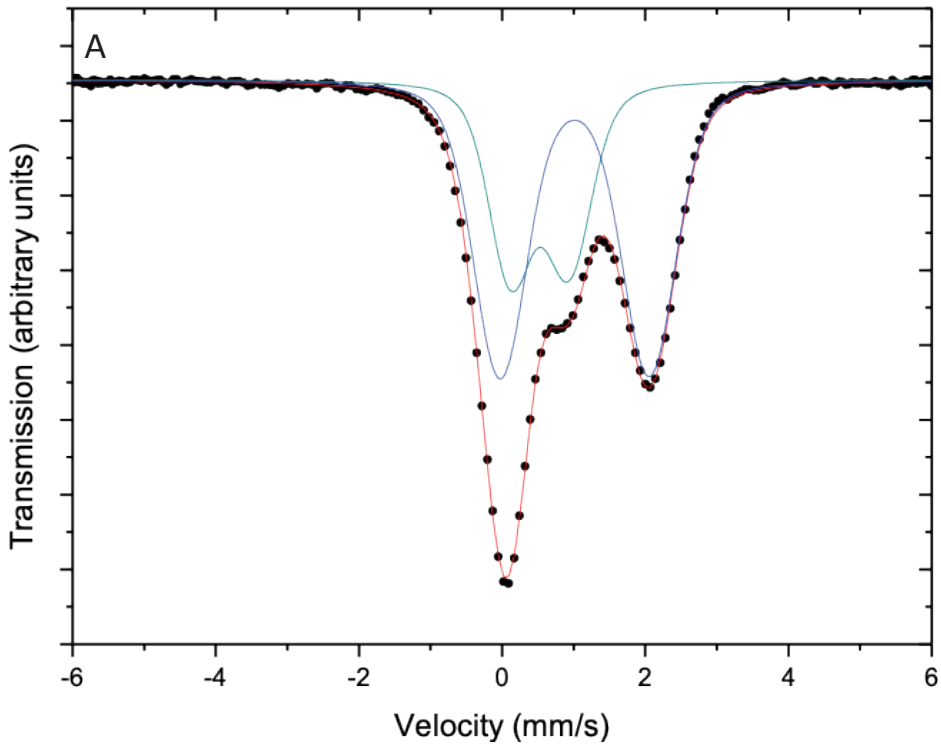


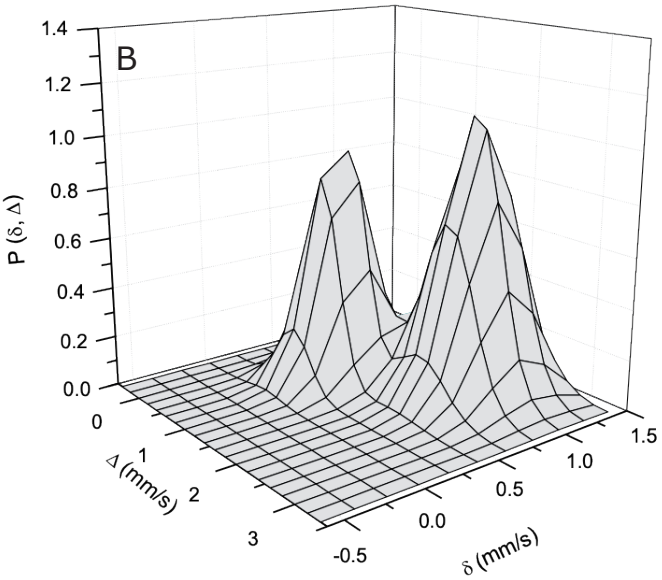


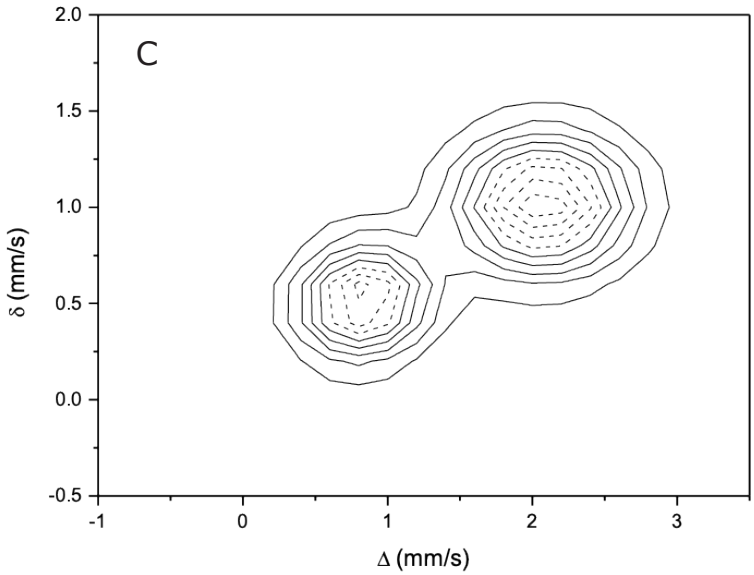

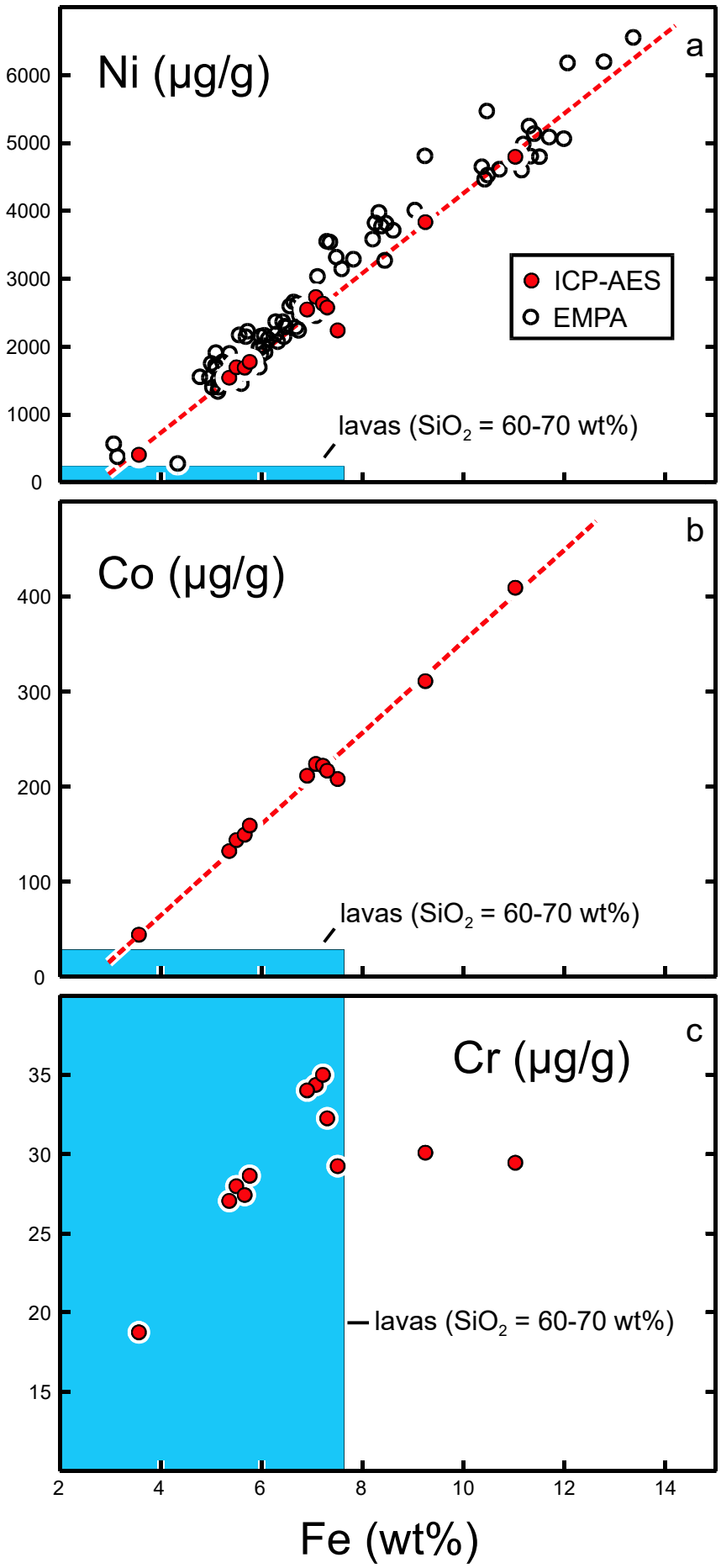

Fig 01 (low resolution)



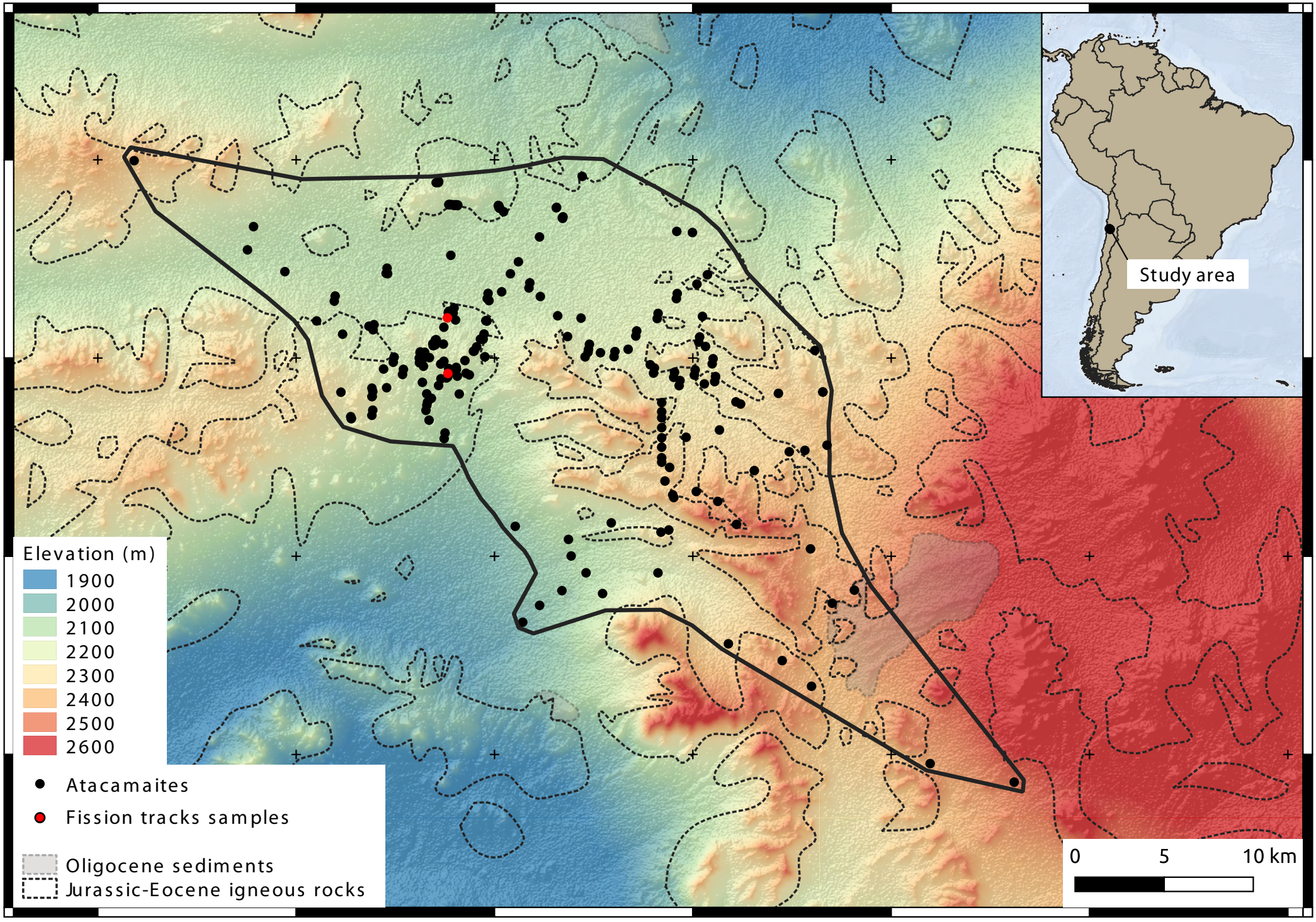

Figure 01 (high-resolution)

Click here to access/download

**Figure (high-resolution)**

Figure 01 revised.pdf